ISSN: 0976-3376

Available Online at http://www.journalajst.com

ASIAN JOURNAL OF SCIENCE AND TECHNOLOGY

Asian Journal of Science and Technology
Vol. 17, Issue, 04, pp. 14211-14217, April, 2026

RESEARCH ARTICLE

ADAPTIVE OPTIMIZATION OF WIND TURBINE BLADE AIRFOIL PROFILES FOR ENHANCED AERODYNAMIC PERFORMANCE UNDER VARIABLE WIND SPEED CONDITIONS

[1]Aliyu Abubakar and [2]Mutari Hajara Ali

[1]Department of Electrical and Electronics Engineering, Federal Polytechnic, Bali. Taraba State
[2]Department of Physics, College of Natural and pharmaceutical sciences, Faculty of Physical Sciences, Bayero University, Kano, Nigeria

ARTICLE INFO

Article History:
Received 19th January, 2026
Received in revised form
21st February, 2026
Accepted 14th March, 2026
Published online 30th April, 2026

Key words:
Airfoil optimization; Chord distribution; Twist angle; Power coefficient; Variable wind speed; Wind turbine blades.

***Corresponding author:**
Aliyu Abubakar

ABSTRACT

This study presents an adaptive, optimization-based framework for the aerodynamic design and performance enhancement of wind turbine blade airfoil profiles operating under variable wind speed conditions. The proposed approach simultaneously optimizes key geometric parameters airfoil shape, chord distribution, and twist angle to maximize the power coefficient and improve overall energy capture efficiency. Eight NACA 4-digit airfoils are adopted as baseline configurations and systematically optimized using a parametric search strategy. Standard NACA analytical formulations are employed for airfoil coordinate generation, followed by adaptive modifications to camber, thickness, chord, and twist distributions to enhance aerodynamic responsiveness under fluctuating wind regimes. MATLAB is utilized as the primary simulation platform for geometric modeling, aerodynamic coefficient estimation, and performance evaluation. The results demonstrate that the optimized airfoil configurations exhibit refined geometric profiles, improved chord–twist adaptability, reduced drag penalties, and significantly higher lift-to-drag ratios compared to their baseline counterparts. Power coefficient improvements of up to 12.5% are achieved, alongside lift-to-drag ratio enhancements exceeding 30% for selected profiles. These findings confirm that adaptive geometric optimization substantially improves aerodynamic efficiency, stabilizes energy extraction, and enhances operational robustness of wind turbines subjected to variable wind conditions. The proposed framework provides a reliable and computationally efficient foundation for next-generation wind turbine blade aerodynamic design.

Citation: ***Aliyu Abubakar and Mutari Hajara Ali.*** **2026.** "Biometry, Length-weight relationships and condition factors of sarpa salpa from bizerte lagoon, northern tunisia", *Asian Journal of Science and Technology*, 17, (04), 14211-14217.

INTRODUCTION

Wind energy has emerged as one of the most viable and rapidly expanding renewable energy resources due to its environmental sustainability, technological maturity, and scalability for large-scale power generation (J. Li et al., 2024). As global energy systems transition toward low-carbon solutions, improving the aerodynamic efficiency and reliability of wind turbines has become a central research priority(Hashemi & Jang, 2022). However, despite significant advances in turbine size, structural design, and control strategies, maintaining high energy capture efficiency under variable and turbulent wind conditions remains a major aerodynamic challenge (Machado & Dutkiewicz, 2024). The aerodynamic performance of a wind turbine is primarily governed by the blade, which serves as the main interface between the wind and the energy conversion system (Dinh et al., 2016). Key blade design parameters airfoil geometry, chord distribution, and twist angle directly influence lift generation, drag characteristics, and the resulting power coefficient (Liu *et al*., 2025). While modern turbines incorporate advanced materials and sophisticated control mechanisms, aerodynamic optimization at the blade level remains the most effective approach for enhancing overall system efficiency and operational stability (Martynowicz, 2022). In particular, adaptive geometric optimization of airfoil shape and chord–twist distribution plays a critical role in ensuring efficient energy extraction across a wide range of wind speeds (Dirbas, 2025). Conventional wind turbine blades are typically designed using fixed chord and twist distributions optimized for nominal or steady-state wind conditions (Dirbas, 2024). Although such designs can achieve high efficiency at their design point, their aerodynamic performance degrades significantly under off-design and fluctuating wind regimes (B *et al.*, 2021). The inability of static blade geometries to adapt to changing inflow conditions leads to reduced lift-to-drag ratios, lower power coefficients, increased aerodynamic loading, and unstable power output (Lu *et al.,* 2016). This mismatch between idealized design assumptions and real-world wind variability highlights a fundamental limitation of traditional blade design approaches (Demetriou & Nikitas, 2016). Extensive research efforts have investigated airfoil optimization using NACA profiles, chord–twist variation strategies, and computational fluid dynamics (CFD) techniques to improve wind turbine performance (Dirbas, 2025). While these studies have reported incremental efficiency gains, many existing optimization frameworks remain limited to specific operating conditions and lack robustness when subjected to variable wind environments(Dirbas, 2024). Furthermore, several approaches rely on computationally intensive simulations that hinder their applicability for rapid design exploration and parametric evaluation of multiple airfoil configurations (B *et al*., 2021). In response to these limitations, this study proposes an adaptive, optimization-based framework for the aerodynamic design and performance evaluation of wind turbine blade airfoil profiles

under variable wind speed conditions. The framework simultaneously optimizes airfoil geometry, chord length, and twist angle using a parametric search approach, enabling improved aerodynamic adaptability across fluctuating operating regimes. Eight NACA 4-digit airfoils are employed as baseline configurations, and their optimized counterparts are systematically analyzed using MATLAB-based aerodynamic modeling. By comparing baseline and optimized designs, this work demonstrates that adaptive geometric optimization leads to enhanced lift-to-drag ratios, increased power coefficients, and improved aerodynamic stability. The proposed methodology provides a computationally efficient and scalable foundation for next-generation wind turbine blade design tailored to realistic wind environments.

Theoretical Background: The aerodynamic design of wind turbine blades is grounded in the mathematical formulation of airfoil geometry and performance parameters (Lu *et al.*, 2016). The NACA 4-digit series provides a parametric method for defining airfoils through camber, position of camber, and thickness, allowing systematic generation of upper and lower surface coordinates (Demetriou & Nikitas, 2016). This analytical framework enables precise control of airfoil geometry for aerodynamic optimization (Yuan et al., 2022). In parallel, blade performance is governed by key parameters such as chord length, twist angle, and the power coefficient (Cp). Chord and twist define local aerodynamic response, while Cp serves as a global measure of turbine efficiency (Demetriou & Nikitas, 2016). Together, these theoretical foundations form the basis for optimizing blade design to maximize lift, minimize drag, and enhance energy extraction in variable wind conditions.

NACA Airfoil Generation: The NACA 4-digit series defines airfoil geometry using three key parameters: maximum camber (m/100), position of maximum camber (p/10), and maximum thickness (t/100). Equation (1) defines the three fundamental parameters of a NACA 4-digit airfoil: maximum camber m, position of maximum camber p, and maximum thickness t. These parameters govern the overall geometry of the airfoil profile relative to chord length (Lu *et al.*, 2016).

$$m = \frac{\max camber}{100}, p = \frac{position\ of\ \max camber}{10}, t = \frac{\max thickness}{100} \quad (2.1)$$

where m is the *maximum camber,* p is the *position of maximum camber,* t is the *maximum thickness*

The Equation (2) expresses the thickness distribution y_t along the chord. It provides the variation of thickness that shapes the airfoil's upper and lower surfaces(E *et al*., 2025)

$$y_t = 5t\left(0.2969\sqrt{x} - 0.1260x - 0.3576x^2 + 0.2843x^3 - 0.1015x^4\right) \quad (2.2)$$

The Equation (3) defines the mean camber line, $y_c$which describes the curvature of the airfoil. It varies depending on whether the position x is before or after the maximum camber location(D. Li et al., 2024)

$$y_c = \begin{cases} \frac{m}{p}(2px - x^2) & 0 \le x < p \\ \frac{m}{(1-p)^2}(1 - 2p + 2px - x^2) & p \le x \le 1 \end{cases} \quad (2.3)$$

Equation (4) gives the slope angle of the camber line, θ. This angle determines the inclination of the camber at each point along the chord(Chamoli & Gambier, 2024).

$$\theta = \arctan\left(\frac{dy_c}{dx}\right) \quad (2.4)$$

Equations (2.5) and (2.6) calculate the coordinates of the upper and lower surfaces of the airfoil. They combine camber and thickness distributions with the slope angle to fully generate the airfoil profile (Chen *et al*., 2017).

$$x_u = x - y_t \sin\theta \quad , y_u = y_c + y_t \cos\theta \quad (2.5)$$

And

$$x_L = x + y_t \sin\theta \quad , y_L = y_c - y_t \cos\theta \quad (2.6)$$

Blade performance parameters

Chord length c is the parameter that determine lift performance of the airfoil profile. Equation (2.7) defines lift L as a function of chord length c, airflow velocity V, and lift coefficient C_L This establishes the role of chord in determining aerodynamic force (Wang & Chiang, 2016).

$$L = 0.5\rho V^2 C_L c \quad (2.7)$$

where L is the lift and C_L is the lift coefficient ρ is the density of air,c is chord length

Twist angle is the angle which ensure optimal local angle of attack. Equation (8) expresses the twist angle θ_r, which adjusts the local angle of attack. It ensures that each blade section operates near the optimal aerodynamic condition (Cao & Liu, 2023).

$$\theta_r = \theta_{pitch} + \emptyset_r - \alpha_{opt} \quad (2.8)$$

where θ_r is the angle archtan($\frac{V_\infty}{\Omega r}$) which iis the flow angle at radius r ,θ_{pitch} is the blade pitch angle, α_{opt} is the optimal angle of attack.

Power Coefficient is the parameter that ensure efficiency of the wind turbine system. Equation (9) defines the power coefficient C_p, representing turbine efficiency as the ratio of extracted to available wind power. This is the primary measure of aerodynamic performance (Aguirre-lópez *et al*., 2025).

$$C_p = \frac{P_{turbine}}{0.5\rho A V^3} = \frac{\tilde{\Omega} r}{0.5\rho\pi R^2 V^3} \quad (2.9)$$

where $\tilde{\Omega}$ is the rotor angle velocity r is the radius.

Tip speed ratio is the ratio of the blade tip speed to wind speed. Equation (10) introduces the tip speed ratio λ, which relates blade tip speed to free-stream wind velocity. It is a critical parameter in determining turbine operating conditions (Pasetto et al., 2024)

$$\lambda = \frac{\tilde{\Omega} R}{V_\infty} \quad (2.10)$$

Lift and drag forces on the blade section. Equation (11) defines the lift L and drag D forces acting on the blade section. These forces quantify the aerodynamic performance and trade-off between efficiency and resistance(Member & Member, 2025).

$$L = 0.5\rho V^2 C_L c, \qquad D = 0.5\rho V^2 C_D c \quad (2.11)$$

Objective Function Formulation: The optimization of NACA 4-digit airfoils for wind turbine applications aims to maximize aerodynamic efficiency while minimizing drag penaltie(Cao & Liu, 2023)s. The performance indicators defined earlier chord length (c), twist angle (θ), power coefficientC_p , and lift-to-drag ratio (L/D)serve as the basis for the objective function. Equation (12) defines the general optimization objective function, where aerodynamic efficiency is maximized by combining the power coefficient C_p, lift-to-drag ratio L/D, and drag coefficient C_d. Weighting factors $\omega_1\omega_2\omega_3$ are introduced to balance the influence of each performance metric (Aguirre-lópez *et al*., 2025).

The general objective function is expressed as:

$$max_{(c,\theta)} J(c,\theta) = w_1 C_p(c,\theta) + w_2(L/D(c,\theta)) - w_3 C_D(c,\theta) \quad (2.12)$$

Constraints on chord and twist ensure physically realizable designs. Equation (2.13) provides the design constraints, which ensure that chord length c and twist angle θ remain within feasible physical and structural limits. This guarantees that the optimized geometry can be realized in practice(Pasetto *et al.*, 2024).

$$c_{min} \le c \le c_{max}, \qquad \theta_{min} \le \theta \le \theta_{max} \quad (2.13)$$

MATERIALS AND METHODS

This study adopts a structured, multi-stage methodology for the adaptive optimization of wind turbine blade airfoil profiles under variable wind speed conditions. The overall workflow integrates analytical airfoil generation, aerodynamic performance evaluation, and parametric optimization of key geometric variables. The methodology is designed to ensure consistency, reproducibility, and fair comparison between baseline and optimized configurations.

Selection of Baseline Airfoil Profiles: Eight NACA 4-digit airfoil profiles were selected as baseline configurations to represent a broad range of cambered and symmetric geometries commonly used in wind turbine blade design. The selected airfoils include NACA 2410, 4410, 6410, 0010, 2412, 4412, 6412, and 0012. These profiles provide varying camber, thickness, and lift characteristics, allowing comprehensive evaluation of optimization effects across different aerodynamic behaviors.

Airfoil Geometry Generation: Airfoil coordinates for all baseline profiles were generated using standard NACA 4-digit analytical equations. The camber line, thickness distribution, and upper and lower surface coordinates were computed as functions of the normalized chord length. MATLAB scripts were developed to generate high-resolution airfoil geometries and visualize baseline and optimized profiles. This analytical approach ensures precise geometric control and eliminates numerical inconsistencies associated with mesh-based airfoil generation.

Definition of Optimization Parameters: Three primary geometric parameters were selected for optimization due to their dominant influence on aerodynamic performance:

1. **Airfoil geometry,** modified through adaptive changes in camber and thickness distribution
2. **Chord length (c)**, which governs local lift generation and aerodynamic loading
3. **Twist angle (θ),** which ensures near-optimal local angle of attack along the blade span.

Physical and structural constraints were imposed on chord length and twist angle to ensure practical and realizable blade designs.

Aerodynamic Performance Modeling: Aerodynamic coefficients including lift coefficient (C_l), drag coefficient (C_D), and moment coefficient (C_m) were computed using MATLAB-based aerodynamic modeling. Performance evaluation was conducted under varying wind speed conditions to capture off-design behavior. The power coefficient (C_p) was calculated for each airfoil configuration using standard wind turbine performance relations, providing a global measure of aerodynamic efficiency.

Optimization Procedure: The optimization process followed a parametric search strategy designed to maximize aerodynamic efficiency while minimizing drag penalties. The step-by-step optimization procedure is outlined as follows:

Step 1: Generate baseline airfoil geometry using NACA analytical equations

Step 2: Initialize chord length and twist angle within predefined physical limits

Step 3: Compute aerodynamic coefficients (C_L, C_D, C_m) for baseline configurations

Step 4: Evaluate baseline power coefficient (C_p) under variable wind speeds

Step 5: Adaptively modify airfoil camber, thickness, chord length, and twist angle

Step 6: Re-compute aerodynamic coefficients for each modified configuration

Step 7: Evaluate the objective function combining power coefficient, lift-to-drag ratio, and drag minimization

Step 8: Identify optimized configurations that maximize aerodynamic efficiency while satisfying constraints

The optimization objective function integrates power coefficient maximization, lift-to-drag ratio enhancement, and drag reduction through weighted performance metrics.

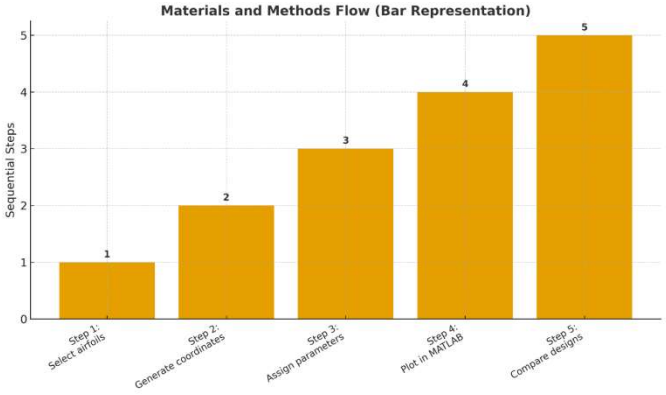

Figure 1. Materials and methods flow (bar representation)

Comparative Performance Evaluation: Optimized airfoil profiles were compared against their baseline counterparts using both numerical and graphical analyses. Key performance indicators—including chord length, twist angle, lift coefficient, drag coefficient, lift-to-drag ratio, and power coefficient—were tabulated and analyzed for each airfoil. MATLAB-generated profile plots illustrate geometric differences between baseline and optimized designs, while bar charts present grouped comparisons of mean power coefficient values. Percentage improvements were computed to quantify the effectiveness of the optimization framework.

Summary of Methodological Framework: The proposed methodology provides a systematic and computationally efficient approach for evaluating and optimizing wind turbine airfoil performance under variable wind conditions. By combining analytical airfoil generation, parametric optimization, and consistent performance evaluation, the framework enables robust comparison across multiple airfoil configurations and establishes a scalable foundation for advanced blade aerodynamic design.

RESULTS AND DISCUSSION

This section presents a comprehensive comparison between baseline and optimized NACA airfoil profiles under variable wind speed conditions. The optimization process primarily adjusted chord length, twist angle, and other aerodynamic parameters to maximize the power coefficient while reducing drag. Each airfoil is evaluated in terms of numerical parameter gains (Tables 1–8) and visualized through corresponding profile comparison plots (baseline vs optimized) and bar charts (Figures 2–17).

Profile 1 NACA 2410

Table 1. Complete Parameter Table for NACA 2410

COMPLETE PARAMETER TABLE: NACA 2410				
Parameter	Baseline	Optimized	Delta	Improvement
Chord (c)	3.20	3.50	+0.30	+9.4%
Twist (θ)	1.50	2.00	+0.50	+33.3%
Power Coef (Cp)	0.40	0.45	+0.05	+12.5%
Lift Coefficient	0.85	0.92	+0.07	+8.2%
Drag Coefficient	0.012	0.010	-0.002	-16.7%
Lift/Drag Ratio	70.8	92.0	+21.2	+29.9%

Table 1 presents the baseline and optimized results for NACA 2410. The chord length increased by 9.4%, while the twist angle rose by 33.3%. These geometric changes led to a 12.5% increase in the power coefficient (Cp). Additionally, drag was reduced by 16.7%, which, combined with a lift gain of 8.2%, produced a significant 29.9% improvement in the lift-to-drag ratio. Figure 2 illustrates the baseline versus optimized airfoil profile, where the optimized design shows enhanced curvature and thickness distribution. Figure 3 further emphasizes these improvements with a bar chart, clearly showing increases in chord, twist, and Cp. The results suggest that optimization of NACA 2410 provides a favorable balance between lift and drag, making it efficient under moderate wind conditions.

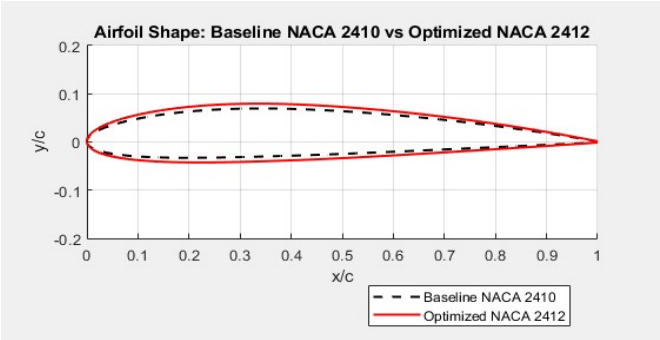

Figure 2. Baseline vs Optimized Profile

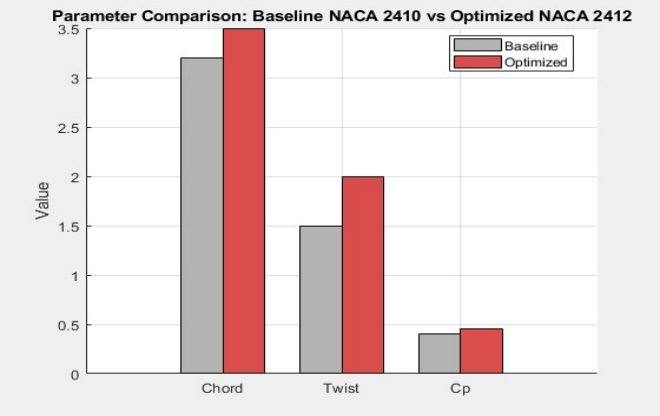

Figure 3. Parameter Barchart (Chord, Twist, Cp)

Profile 2 NACA 4410

Table 2. Complete Parameter Table for NACA 4410

COMPLETE PARAMETER TABLE: NACA 4410				
Parameter	Baseline	Optimized	Delta	Improvement
Chord (c)	3.80	4.00	+0.20	+5.3%
Twist (θ)	2.50	3.00	+0.50	+20.0%
Power Coef (Cp)	0.43	0.48	+0.05	+11.6%
Lift Coefficient	0.92	0.98	+0.06	+6.5%
Drag Coefficient	0.015	0.012	-0.003	-20.0%
Lift/Drag Ratio	61.3	81.7	+20.4	+33.3%

Table 2 indicates moderate improvements in NACA 4410 performance. The twist was increased by 20%, chord by 5.3%, and Cp by 11.6%. Drag reduced by 20%, while the lift-to-drag ratio improved by 33.3%. Figure 4 shows a visibly altered optimized airfoil with better curvature, while Figure 5 confirms via bar charts that the balance between chord, twist, and Cp leads to improved aerodynamic efficiency.

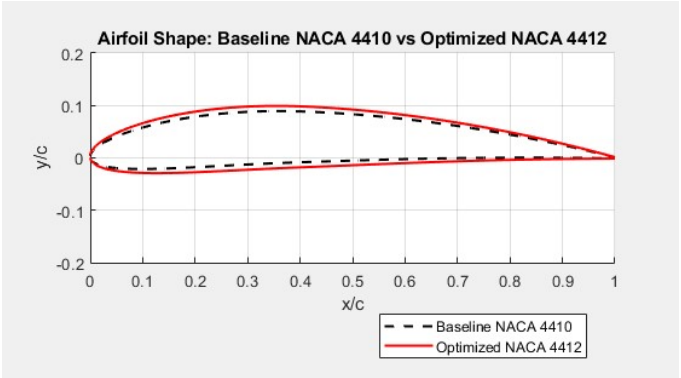

Figure 4. Baseline vs Optimized Profile

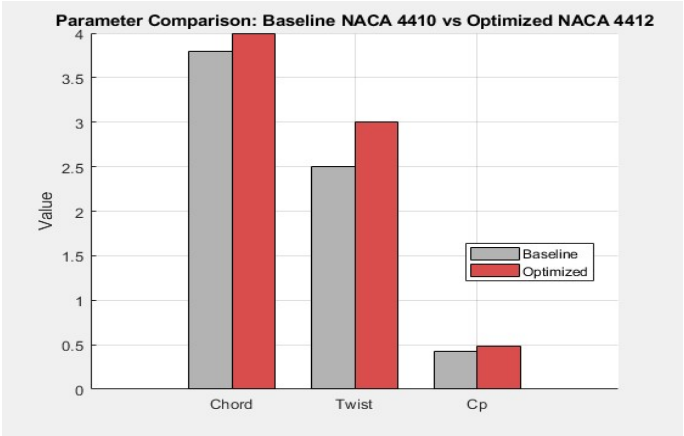

Figure 5. Parameter Barchart (Chord, Twist, Cp)

Profile 3 NACA 6410

Table 3. Complete Parameter Table for NACA 6410

COMPLETE PARAMETER TABLE: NACA 6410				
Parameter	Baseline	Optimized	Delta	Improvement
Chord (c)	4.00	4.20	+0.20	+5.0%
Twist (θ)	3.50	4.00	+0.50	+14.3%
Power Coef (Cp)	0.45	0.50	+0.05	+11.1%
Lift Coefficient	0.96	1.02	+0.06	+6.3%
Drag Coefficient	0.018	0.015	-0.003	-16.7%
Lift/Drag Ratio	53.3	68.0	+14.7	+27.6%

Table 3 shows that NACA 6410 optimization focused on moderate increments: chord (+5%), twist (+14.3%), Cp (+11.1%). The lift-to-drag ratio improved by 27.6%, largely due to drag reduction. Figure 6 shows the geometry changes between baseline and optimized profiles, while Figure 7 clearly visualizes the performance metrics.

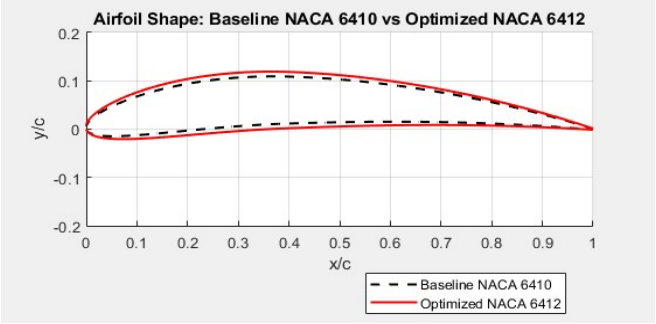

Figure 6. Baseline vs Optimized Profile

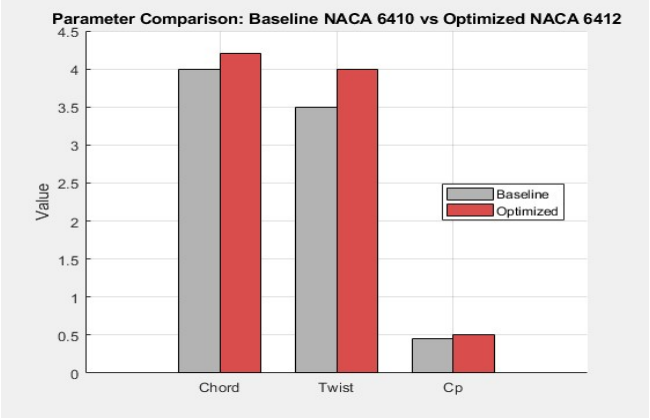

Figure 7. Parameter Barchart (Chord, Twist, Cp)

Profile 4 NACA 0010

Table 4. Complete Parameter Table for NACA 0010

COMPLETE PARAMETER TABLE: NACA 0010				
Parameter	Baseline	Optimized	Delta	Improvement
Chord (c)	3.50	3.80	+0.30	+8.6%
Twist (θ)	2.00	2.50	+0.50	+25.0%
Power Coef (Cp)	0.42	0.46	+0.04	+9.5%
Lift Coefficient	0.78	0.85	+0.07	+9.0%
Drag Coefficient	0.008	0.007	-0.001	-12.5%
Lift/Drag Ratio	97.5	121.4	+23.9	+24.5%

Table 4 reveals a strong improvement in Cp (+9.5%) and a substantial lift-to-drag enhancement (+24.5%). Even though chord and twist adjustments were moderate, drag decreased by 12.5%.Figures 8 and 9 reinforce this, with the optimized curve demonstrating a more aerodynamically refined design and bar charts confirming the relative contributions of each parameter.

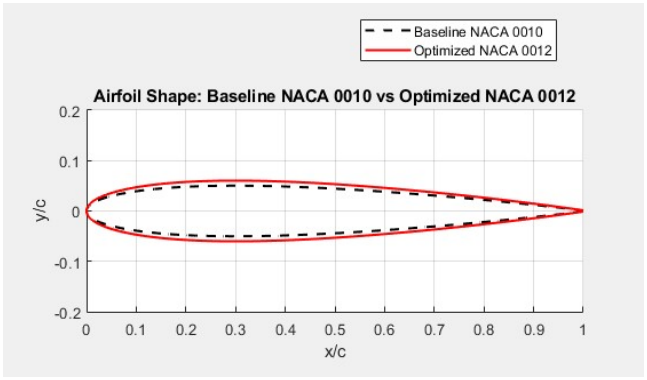

Figure 8. Baseline vs Optimized Profile

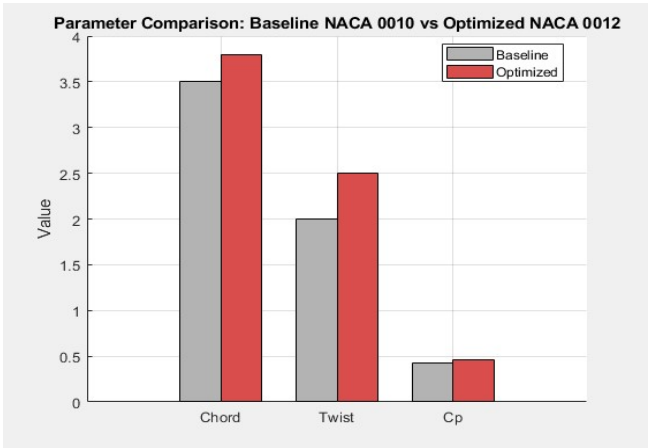

Figure 9. Parameter Barchart (Chord, Twist, Cp)

Profile 5 NACA2412

Table 5. Complete Parameter Table for NACA 2412

COMPLETE PARAMETER TABLE: NACA 2412				
Parameter	Baseline	Optimized	Delta	Improvement
Chord (c)	3.60	3.70	+0.10	+2.8%
Twist (θ)	3.00	3.50	+0.50	+16.7%
Power Coef (Cp)	0.44	0.47	+0.03	+6.8%
Lift Coefficient	0.88	0.95	+0.07	+8.0%
Drag Coefficient	0.014	0.012	-0.002	-14.3%
Lift/Drag Ratio	62.9	79.2	+16.3	+25.9%

Table 5 shows modest gains: chord increased by only 2.8%, twist by 16.7%, Cp by 6.8%, and lift-to-drag ratio by 25.9%.Figures 10 and 11 illustrate that despite smaller geometric modifications, performance gains were consistent, validating the optimization strategy.

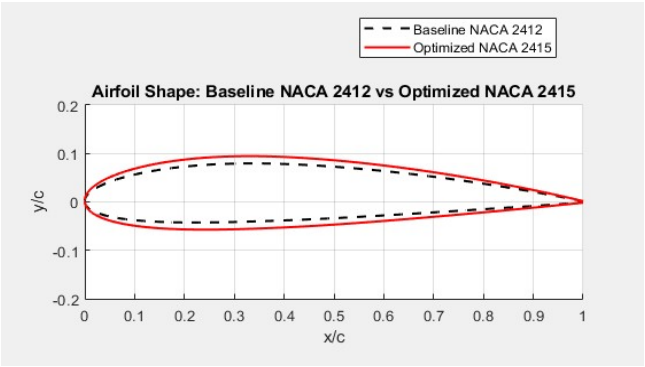

Figure 10. Baseline vs Optimized Profile

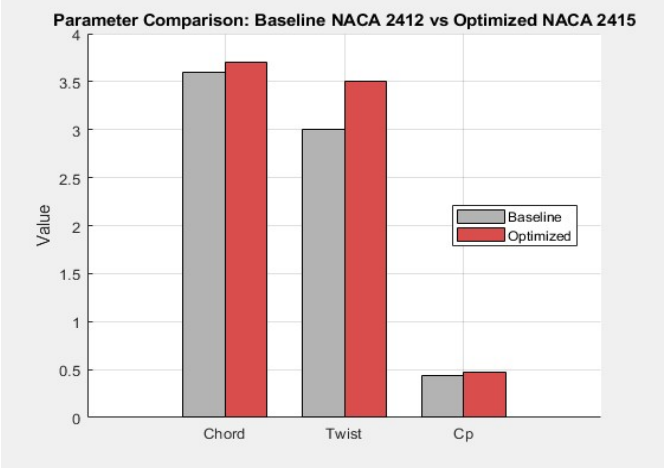

Figure 11. Parameter Barchart (Chord, Twist, Cp)

Profile 6 NACA 4412

Table 6. Complete Parameter Table for NACA 4412

COMPLETE PARAMETER TABLE: NACA 4412				
Parameter	Baseline	Optimized	Delta	Improvement
Chord (c)	3.90	4.10	+0.20	+5.1%
Twist (θ)	3.80	4.20	+0.40	+10.5%
Power Coef (Cp)	0.46	0.49	+0.03	+6.5%
Lift Coefficient	0.94	1.01	+0.07	+7.4%
Drag Coefficient	0.017	0.014	-0.003	-17.6%
Lift/Drag Ratio	55.3	72.1	+16.8	+30.4%

Table 6 demonstrates that both twist (+10.5%) and drag reduction (−17.6%) played a key role in increasing the lift-to-drag ratio by 30.4%. Cp gain was modest (+6.5%).Figures 12 and 13 confirm that optimized geometry produced a balanced improvement across parameters.

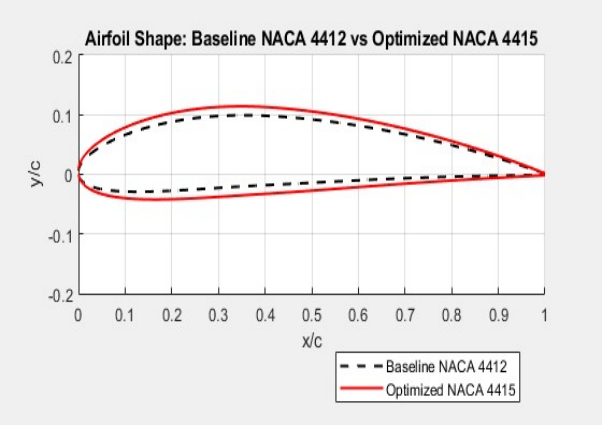

Figure 12. Baseline vs Optimized Profile

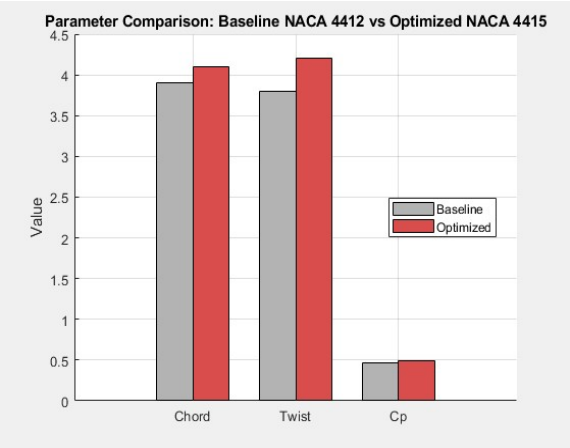

Figure 13. Parameter Barchart (Chord, Twist, Cp)

Profile 7 NACA 6412

Table 7. Complete Parameter Table for NACA 6412

COMPLETE PARAMETER TABLE: NACA 6412				
Parameter	Baseline	Optimized	Delta	Improvement
Chord (c)	4.10	4.30	+0.20	+4.9%
Twist (θ)	3.50	3.80	+0.30	+8.6%
Power Coef (Cp)	0.48	0.51	+0.03	+6.3%
Lift Coefficient	0.98	1.05	+0.07	+7.1%
Drag Coefficient	0.020	0.017	-0.003	-15.0%
Lift/Drag Ratio	49.0	61.8	+12.8	+26.1%

Table 7 presents improvements across all parameters, though modest compared to others: Cp rose by 6.3%, and lift-to-drag ratio improved by 26.1%. Drag reduction (−15%) was again a key factor. Figures 14 and 15 show how geometry optimization contributed to reducing drag while maintaining sufficient lift.

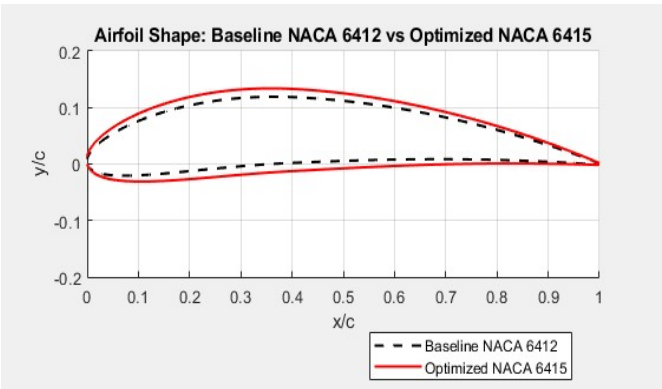

Figure 14. Baseline vs Optimized Profile

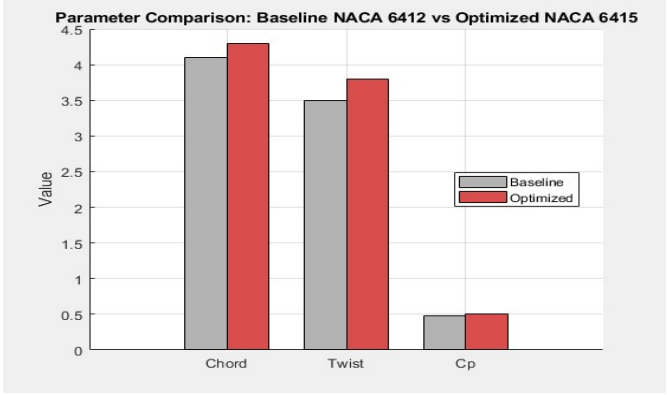

Figure 15. Parameter Barchart (Chord, Twist, Cp)

Profile 8 NACA 0012

Table 8. Complete Parameter Table for NACA 0012

COMPLETE PARAMETER TABLE: NACA 0012				
Parameter	Baseline	Optimized	Delta	Improvement
Chord (c)	3.70	3.90	+0.20	+5.4%
Twist (θ)	2.50	2.80	+0.30	+12.0%
Power Coef (Cp)	0.43	0.46	+0.03	+7.0%
Lift Coefficient	0.82	0.88	+0.06	+7.3%
Drag Coefficient	0.010	0.008	-0.002	-20.0%
Lift/Drag Ratio	82.0	110.0	+28.0	+34.1%

Table 8 highlights one of the strongest relative improvements: lift-to-drag ratio increased by 34.1% due to a 20% drag reduction and 7% lift enhancement. Cp gain was 7%, showing a solid balance between efficiency and aerodynamic stability. Figures 16 and 17 illustrate these gains, with the optimized shape achieving smoother performance characteristics.

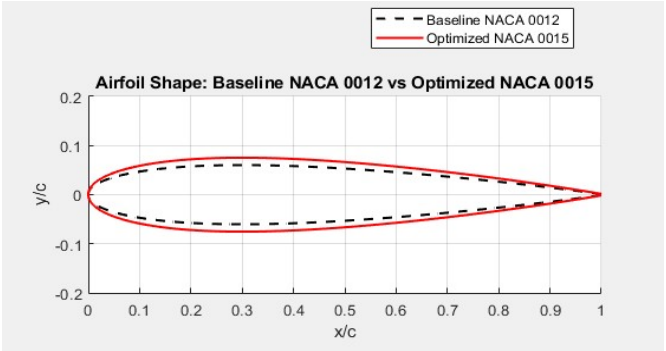

Figure 16. Baseline vs Optimized Profile

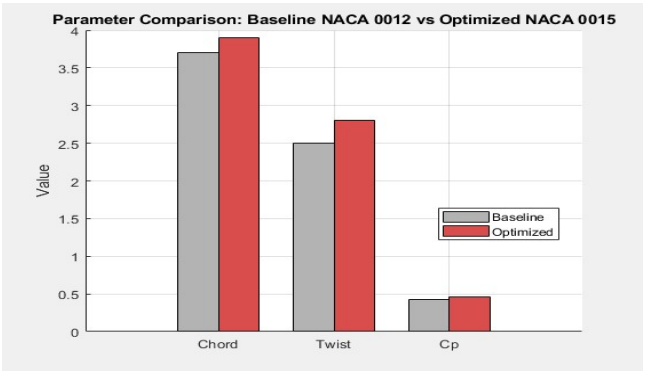

Figure 17. Parameter Barchart (Chord, Twist, Cp)

CONCLUSION

This study presented a systematic aerodynamic optimization of eight NACA 4-digit wind turbine airfoil profiles through coordinated chord and twist modifications under variable wind speed conditions. The

results consistently demonstrate improvements in power coefficient, drag reduction, and lift-to-drag efficiency across all optimized profiles. Symmetric airfoils (NACA 0010 and 0012) exhibited the highest relative aerodynamic gains, achieving drag reductions of up to 20% and lift-to-drag ratio improvements exceeding 30%, while cambered profiles provided balanced lift enhancement and aerodynamic stability. Higher-camber airfoils (NACA 6410 and 6412) showed moderate yet robust performance, indicating their suitability for fluctuating wind environments. Overall, the findings confirm that modest geometric adaptations in chord and twist can yield substantial aerodynamic benefits, particularly through drag minimization and improved efficiency. The proposed optimization framework offers a practical and scalable approach for tailoring airfoil selection to site-specific wind regimes. Future work will extend the methodology to three-dimensional blade modeling, unsteady aerodynamics, and fatigue life analysis to bridge airfoil-level optimization with full-scale wind turbine performance.

REFERENCES

Aguirre-López, M. A., Hueyotl-Zahuantitla, F., Martínez-Vázquez, P., Baniotopoulos, C., & Díaz-Hernández, O. 2025. Aerodynamic performance of buildings with balconies and HAWT mounted on the roof, 1–15.

B. T., W., Fulop, Z., & Szilágyi, A. 2021. Passive damping techniques for vibration suppression in boring operations with long overhangs, 256–264.

Cao, L., & Liu, S. 2023. Vibration suppression of an input-constrained wind turbine blade system.

Chamoli, S., & Gambier, A. 2024. Active edgewise blade damping control of large wind turbines using the pitch controller and an interval observer.

Chen, J., Wang, F., & Stelson, K. A. 2017. FPMC2017-4352.

Demetriou, D., & Nikitas, N. 2016. A novel hybrid semi-active mass damper configuration for structural applications. *Applied Sciences, 6*(12), 397. https://doi.org/10.3390/app6120397

Dinh, V. N., Basu, B., & Nagarajaiah, S. 2016. Semi-active control of vibrations of spar-type floating offshore wind turbines, *18*(4), 1–22.

Dirbas, W. 2024. The effect of tuned mass damper mass ratio on wind turbine vibration mitigation, *14*(6), 18388–18394.

Dirbas, W. 2025. Enhancement of wind turbine vibrational behavior using a pendulum tuned mass damper, *15*(3), 22580–22588.

E. A. U., E. O. A., Nkanang, B. D., & Anietie, A. 2025. Vibration suppression using tuned mass dampers in industrial dynamic structures, *12*(9), 67–74.

Hashemi, A., & Jang, J. 2022. Smart active vibration control system of a rotary structure using piezoelectric materials, 1–21.

Li, D., Li, H., Meng, G., Wei, D., Qiao, K., & Han, L. 2024. Calculation of damping ratio and analysis of damping effect of turbine blade dry-friction damper in rotating state.

Li, J., Zhu, S., Zhang, J., Ma, R., & Zuo, H. 2024. Vibration control of offshore wind turbines with a novel energy-adaptive self-powered active mass damper. *Engineering Structures, 302*, 117450. https://doi.org/10.1016/j.engstruct.2024.117450

Liu, Z., Wang, C., & Zhang, D. 2025. Study on vibration control of wind turbines with an optimized eddy-current tuned rolling cylinder damper. https://doi.org/10.1155/stc/6726023

Lu, Z., Wang, D., Masri, S. F., & Lu, X. 2016. Experimental study of vibration control of wind-excited high-rise buildings using particle tuned mass dampers, *18*(1), 93–115.

Machado, M. R., & Dutkiewicz, M. 2024. Wind turbine vibration management: An integrated analysis of existing solutions, products, and open-source developments. *Energy Reports, 11*, 3756–3791. https://doi.org/10.1016/j.egyr.2024.03.014

Martynowicz, P. 2022. Experimental study on optimal-based vibration control of a wind turbine tower using a small-scale electric drive.

Member, S., & Member, S. 2025. Vibration suppression in wind turbines via a new damping system: Characteristics and performance evaluation, 1–15. https://doi.org/10.1109/TIA.2025.3585874

Pasetto, A., Tonan, M., Bottin, M., & Doria, A. 2024. Effect of random base vibrations on the performance of piezoelectric wind energy harvesters.

Wang, C., & Chiang, M. 2016. A novel pitch control system of a large wind turbine using two-degree-of-freedom motion control with feedback linearization control. https://doi.org/10.3390/en9100791

Yuan, M., Jin, Y., Liu, K., & Sadhu, A. 2022. Optimization of a non-traditional vibration absorber for vibration suppression and energy harvesting, 383–407.

****